Liverpool Telescope Technical Note 1: Telescope and IO:O Throughput

Abstract: We measure the absolute photon efficiency of the Liverpool Telescope using observations of photometric standard stars and a throughput model of the IO:O instrument. Over a period of 1 year following mirror re-coating the telescope transmission is in the range 73–79% over 4000–10000Å. Transmission in the u'-band (~ 3500Å) is slightly lower at 65%. Immediately following mirror re-coating the throughput is shown to be consistent within 4% to predictions for two reflections from bare-aluminium-coated optics. The telescope throughput (two reflections) degrades at a rate $\approx 0.0002\,\mathrm{mag\,day^{-1}}$. Also presented are the effective wavelengths and widths for the u', g', r', i', z', B, V broad-band filters, taking into account all optical components of the system.

R.J. Smith, I.A. Steele

v1.0

February 16, 2017

1 Summary of Results

The telescope throughput was measured using observations of standard stars with the IO:O camera, taking into account the characteristics of the CCD quantum efficiency, filter transmission, cryostat window transmission and the telescope effective area. The results are summarized in Table 1.

Band	Effective Wavelength (Å)	Bandpass (Å)	Telescope Throughput (%)	IO:O Efficiency (%)
u'	3476	250	65	37
B	4416	434	78	46
g'	4853	971	79	65
V	5398	647	75	75
r'	6197	1152	77	89
i'	7636	1188	73	86
z'	9006	784	76	38

Table 1: Measured telescope throughput (primary and secondary mirrors) and IO:O efficiency (incorporating detector QE, window transmission and filter transmission) as a function of the effective wavelength of the IO:O filters. The telescope effective area is 2.5133 m^2.

Details of the analysis are presented in Sections 2–6 below.

2 Methodology

The sensitivity of a telescope/instrument combination is generally measured in terms of the natural instrumental *Zero Point*. This is the magnitude of a star which provides one detected photo-electron per second. In order to convert this to an absolute throughput as a per cent of the incoming flux, we need to know the absolute incoming photon flux and make allowances for all other photon losses; atmosphere, filters, detector QE etc. Since the photometric measurements are performed by the complete system (telescope and instrument), all these components need to be included in the analysis. For this study we use the IO:O camera. This means rather than just the telescope efficiency, this document must cover both telescope and IO:O efficiency. The results are presented both as a measured throughput for the complete telescope-plus-IO:O system and for the telescope alone once a model for losses in the IO:O instrument have been added back in.

The full system zero point (including telescope, atmosphere, instrument) is determined from observations of standard stars. We used the secondary standard star network established by the SDSS Calibration Telescope[1]. Since this is based on an AB magnitude system, all the u', g', r', i', z' filters by definition give a flux density of 3631 Jy for a magnitude zero star at the top of the atmosphere. This means a zero magnitude star provides

$$\mathrm{F}_0 = 3631\ (1.51 \times 10^7)\ \frac{\Delta\lambda}{\lambda_0}$$

photons per second incident on one square metre above the atmosphere where λ_0 is the effective wavelength of the filter and $\Delta\lambda$ is the pass-band width.[1]

The strategy we follow is to:

[1] Practical details in the initial establishment of the SDSS reference frame[2] mean small corrections (< 0.04 mag) need to be applied and the zero points for u' and z' are not quite 3631 Jy.

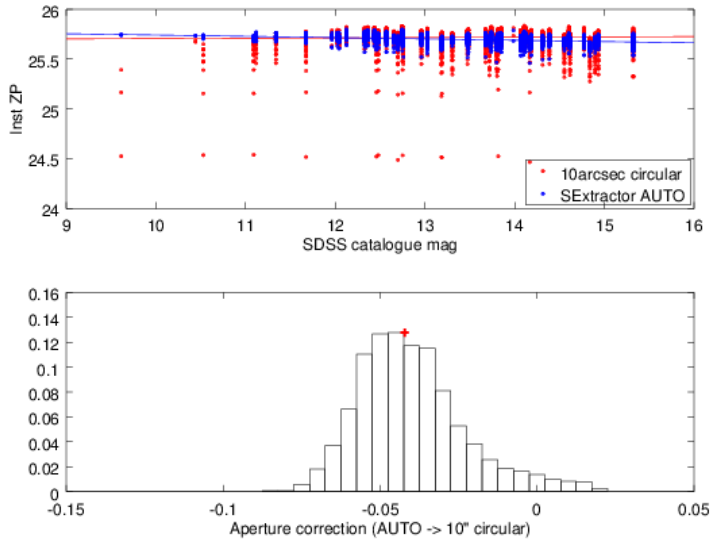

Figure 1: Upper panel compares raw instrumental magnitudes from the two extraction strategies. Compared to large, fixed diameter apertures, the automatic isophotal ellipses do a good job of including the entire flux of the object with an obviously much smaller scatter. The slope of the linear fit to the data reveals $< 5\%$ non-linearity to the isophotal photometry extractions. This is however unimportant because observations of many stars are averaged to give an effective overall zero point for the system and corrected via an aperture correction to match the large aperture extractions. The lower panel is a histogram of the magnitude differences between the two methods, used to derive the aperture correction, matching the mean zero point from the two methods.

- measure the one photo-electron per second zero point (ZP) for each filter by comparison to the SDSS standards,
- derive the photon count rate (airmass = 0) which we would observe through our optical system for a zero magnitude star,
- convert to flux density,
- compare to the expected value of 3631 Jy.

This gives the end-to-end efficiency of the entire instrument and telescope optical system and can be broken down further to investigate the contribution of each component. The following factors are all spectrally sensitive and were directly measured by their respective manufacturers as a function of wavelength:

- Detector QE ,
- Filter pass-bands,
- Cryostat window transmission.

All remaining throughput losses may then be attributed to reflectivity of the telescope mirrors.

3 Photometry

The IO:O instrument has a full set of SDSS style u', g', r', i', z' filters and an incomplete set of Bessell filters (B and V). Five fields of photometric standards (Table 2) are automatically observed by the LT scheduler

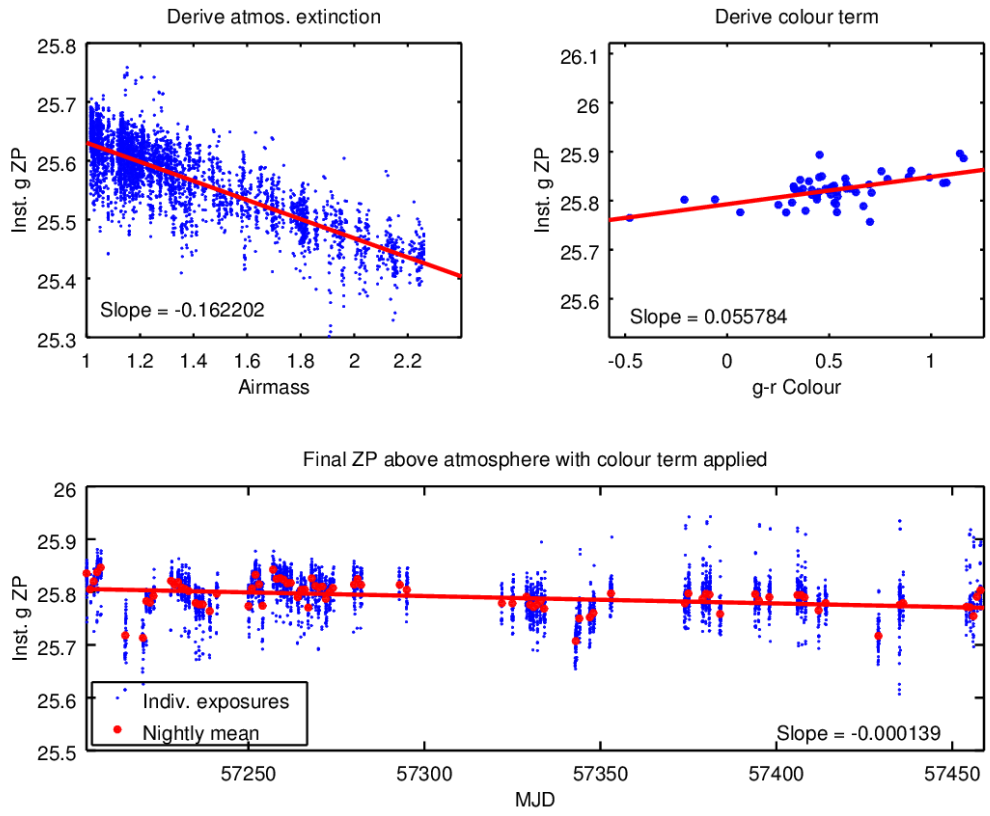

Figure 2: Derivation of the colour, extinction and mirror degradation corrections which were performed independently for each filter. Here the g'-band data are illustrated.

on every night expected to be photometric. All fields were drawn from the SDSS secondary standards network. Three are also covered by the Landolt equatorial fields and are thus appropriate for use with the Bessell filters.

Name	Equatorial Coordinates (J2000)	N_{SDSS}	N_{BV}
SA94_702	02:58:08.49 +01:10:56.0	9	2
SA114_654	22:41:33.40 +01:08:51.8	9	5
PG1047	10:50:10.60 −00:02:06.7	11	10
BD+18_17	17:35:22.60 +18:53:43.1	18	0
LHS_1858	06:37:13.50 +17:34:54.0	15	0

Table 2: Summary of the routinely observed LT photometric fields. Also listed is the typical number of reference stars per observation that fall within the IO:O field of view.

Reference magnitudes in the SDSS system (m_{sdss}) were taken from SDSS[1, 3, 4]. For Bessell B, V filters, we use the magnitudes from the Stetson observations[5] of the Landolt equatorial fields[6]. Stetson provides magnitudes for many more stars per field rather than the small subset selected by Landolt. Where both authors provide a magnitude, they typically agree to better than 0.002 mag. Other than this, the B, V data were handled the same as u', g', r', i', z' and will not generally be discussed as a separate case. The zero magnitude flux densities for the Bessell filters were taken as 4130 Jy for B and 3781 Jy for V[7, 8].

Filter	Atmosphere *(mag/airmass)*	Colour	Coatings *(mag/day)*	$\langle ZP \rangle$	ZP_0
u'	-0.555	$-0.031(u'-g')$	-0.000442	24.53	24.55
g'	-0.164	$+0.057(g'-r')$	-0.000159	25.80	25.81
r'	-0.100	$-0.024(g'-r')$	-0.000236	25.70	25.72
i'	-0.050	$+0.000(r'-i')$	-0.000128	25.44	25.46
z'	-0.040	$-0.237(i'-z')$	-0.000058	24.84	24.86
B	-0.222	$+0.052(B-V)$	-0.000245	25.16	25.19
V	-0.133	$-0.083(B-V)$	-0.000172	25.24	25.26

Table 3: The measured LT photometric calibration parameters. The second through fourth columns tabulate the measured fit slopes in LT data, illustrated for g' in Figure 2. 'Coatings' in the fourth column accounts for any long term temporal drift but is believed to primarily relate to tarnishing of the mirrors' unprotected aluminium coating. $\langle ZP \rangle$ is the derived LT and IO:O system zero point for the nine months covered in this analysis and the final column, ZP_0, is the same value having used the mirror tarnish estimate to project back to the zero point immediately after mirrors were re-coated.

For this study we selected all observations over nine months from 2015 July 01 (mirror recoating) until 2016 March 10. Data were inspected by eye and rejected if any of the frames on that night showed obvious cloud.

The photometry is based on `SExtractor` automatic isophotal ellipse counts plus an aperture correction derived from large (10 arcsec diameter) circular apertures. This combines the advantages of capturing the total flux of large apertures with the lower noise of small apertures while being adaptive enough to handle varying seeing conditions and PSF. As illustrated in Figure 1 there is a small difference between the circular and isophotal apertures as a function of target brightness. This effect is relatively small (≈ 0.05 mag) and not important as we use the ensemble average zero point from all the stars observed on any given night.

Raw instrumental magnitude is defined as

$$m_{inst} = -2.5 \log_{10}\left(\frac{\texttt{ADU} \times \texttt{GAIN}}{\texttt{EXPTIME}}\right) - 0.04$$

where `ADU` is the `SExtractor AUTO` isophotal ellipse counts, `GAIN` = 1.755 electrons per count (measured by the photon transfer curve method on 2014 January 24), `EXPTIME` is the exposure integration time in seconds and 0.04 is the aperture correction that matches the isophotal apertures to the 10 arcsec circular aperture.

Atmospheric extinction corrections were applied on a per image basis according to the airmass of each observation. A single typical extinction value was derived for each filter by a linear fit to a plot of $m_{sdss} - m_{inst}$ vs. $airmass$ for our entire data sample. The top-left panel of Figure 2 illustrates the measured g'-band extinction of 0.16 magnitudes per airmass.

Colour correction transformations were also derived from our data (top-right panel of Figure 2) and applied in order to correct between our filter bands and the reference catalogues' optical systems. For the SDSS-style filters these corrections are small except z' for which the red cutoff is defined by the CCD, not the filter[2].

By applying all the above corrections, for every individual observation we calculate an inferred zero

[2]IO:O uses an e2V deep depletion CCD compared to the thinned SITe chip on the SDSS calibration telescope.

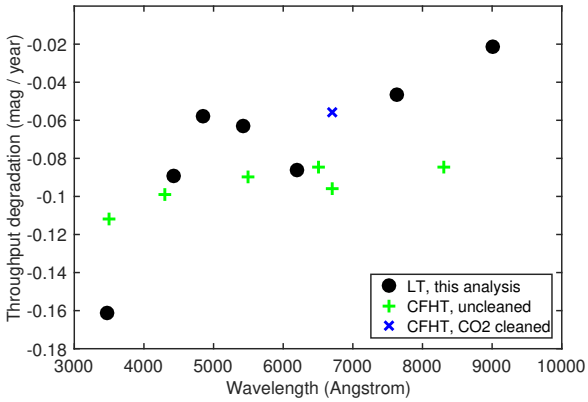

Figure 3: Measured rate at which the IO:O system zero point decays over time. Included for comparison are direct reflectometer measurements of two CFHT coating witness samples[10] which were stored exposed in the enclosure with and without routine CO_2 snow cleaning. The CFHT reflectance data have here been scaled to show the effect of two refections.

point. This zero point is the magnitude of a star that would yield 1 photo-electron per second in the detector above the atmosphere (i.e., airmass = 0).

All observations were then combined into a final system zero point through a two-step process. Firstly a nightly average was obtained as a sigma-clipped mean of all the measurements on each single night. This allows detection and rejection of poor nights which were not previously identified. These could for example have been nights of severely dusty atmosphere. The nightly average zero points are illustrated as large red dots in the lower panel of Figure 2. Secondly, after rejecting the most severe outliers, the final zero point was taken as the median of the set of nightly averages.

Since the observations cover a substantial time range, it is also possible to detect a small temporal decline in total system throughput. We attribute this primarily to tarnishing and dust accumulation on the mirrors' aluminium coating, but could in principle also include contributions from dust accumulation on, or degradation of, any optical surface. This is illustrated in the lower panel of Figure 2 which shows the inferred g' zero point decays at a rate of 0.00016 magnitudes per night. Figure 3 shows how the mirror surface degradation varies with wavelength. The calibration presented here represents the average telescope throughput over the nine months analysed.

4 Conversion to Flux Density

The zero point gives the photon count rate for a zero magnitude star as $10^{0.4\mathrm{ZP}}$. This can be converted to flux density by applying the energy per photon and scaling from the telescope collecting area to one square metre. Geometric collecting area is constant for all filters and discussed in Sec 4.1. Estimating energy per photon requires modeling the spectral response of each instrument component. These components are detailed in Sections 4.2.1 through 4.2.3.

4.1 Collecting area and geometric obstruction

The telescope effective collecting area is the primary mirror area minus obscuration by the secondary and other mechanical structures. The primary mirror has an outer circumference area of $\pi\,\mathrm{m}^2$, but part of that

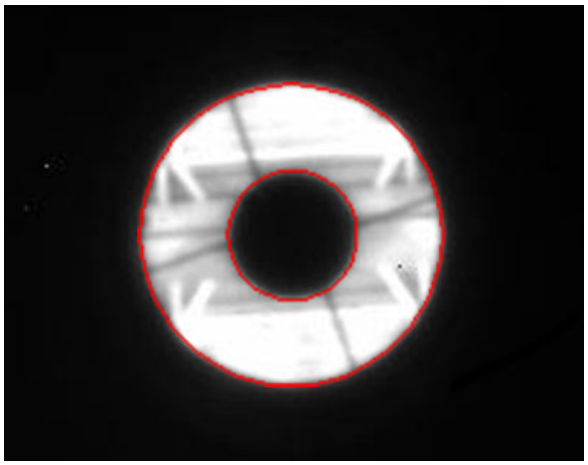

Figure 4: View of the primary mirror with a pinhole camera at the instrument plane, obtained Nov 2007 after the baffles were redesigned and updated. The cross of the secondary support vanes is visible and the rest of the structure visible in the mirror is reflection of steelwork on the interior of the enclosure dome. The inner and outer diameters of the active collecting area were defined as the point where the image brightness was 50% of the mean mirror surface brightness and are marked with red rings. The ratio of inner to outer diameter is 0.423, precisely as defined in the optical design.

is obstructed by the secondary mirror structure; both the baffle around the mirror itself and the spider vanes that support it. The optical design includes a central obstruction with outer diameter of 846mm which is a factor 846/2000 = 0.423 of the diameter or 17.9% of the area of the primary. Including the support vanes increases this to 18.5%. There is also a small amount of obstruction from thick cables (such as the earthing strap that runs along the spider vanes and the SkycamZ camera, giving a total estimate of aperture obstruction as 20% and the effective telescope collecting area is 2.5133 m^2.

As a check we can measure the central obstruction directly from images taken of the interior of the telescope with a pinhole camera mounted at the instrument plane. Because a pinhole camera has effectively infinite depth of field, the entire interior structure of the telescope is visible and the angular diameters of the primary mirror and the secondary mirror baffle can be measured directly. They precisely match the optical design of 17.9% in area. The pinhole camera did not offer sufficient angular resolution to measure the smaller obstructions which contribute to our total estimated obstruction of 20%.

4.2 Components of the pass-bands' spectral model

The effective wavelength for a single filter is defined as the throughput weighted average wavelength,

$$\lambda_0^{\mathrm{filter}} = \frac{\int S\lambda \, d\lambda}{\int S \, d\lambda}$$

where S is the response curve of the filter alone. Similarly the effective wavelength (λ_0) of the entire instrument is given by

$$\lambda_0 = \frac{\int S \, Q \, W \lambda \, d\lambda}{\int S \, Q \, W \, d\lambda}$$

where Q and W are the response curves of the CCD and cryostat windows respectively.

The effective width ($\Delta\lambda$) is the width of a hypothetical perfect top-hat filter with 100% transmission and passing the same total flux. This is simply the divisor of the above formulae for λ_0.

$$\Delta\lambda = \int S\,Q\,W\,d\lambda$$

As previously stated a zero AB magnitude star will by definition provide $F_0^{\rm ref}$=3631 Jy at the top of the atmosphere. The apparent flux density for a zero magnitude star in the LT observations is given by

$$F_0^{\rm LT} = \frac{10^{0.4ZP}\lambda_0}{(1.51\times10^7)(\rm Collecting\_Area)(\Delta\lambda)}$$

with the telescope collecting area expressed in square metres and the pass band descriptors (λ_0, $\Delta\lambda$) in Angstroms.

4.2.1 CCD Quantum Efficiency

The detector is a CCD231-84 (BI, NIMO, deep depletion silicon, Astro ER1 coating) from e2V. The manufacturer provides an illustrative 'typical' quantum efficiency (QE) curve for the detector type along with bench tests of our specific device's absolute QE at five discrete wavelengths 3500 – 9000 Å.

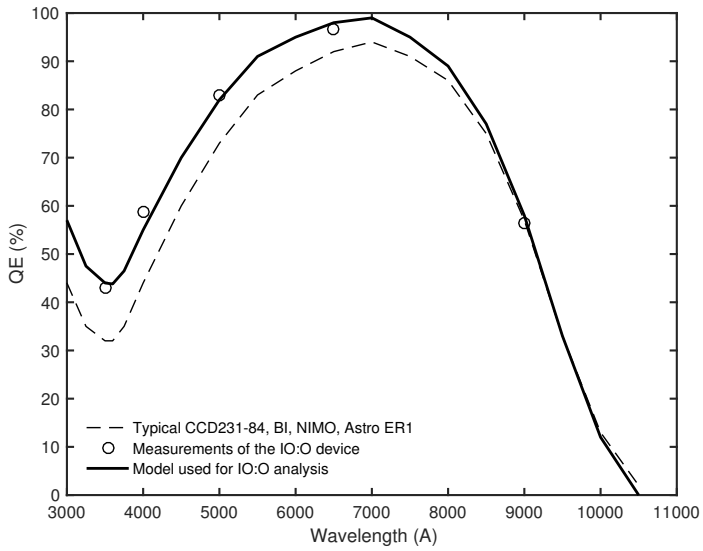

Figure 5: The IO:O detector QE curve showing monochromatic measurements and continuum model.

For the analysis here we created a model of the full QE curve for our detector by taking the 'typical' curve for the type of device and adjusting it to pass through the five spot measurements of our actual device. The resulting model (Figure 5) required only a linear tilt of the QE curve by a few per cent towards the blue to fit the data.

4.2.2 Cryostat Window

The IOO cryostat window is a plano-concave fused silica glass field flattener optic with a custom broadband anti-reflection (AR) coating designed by Asahi Spectra which provides $> 98\%$ transmission from

3230 – 10460 Å. The measured transmission is shown in Figure 6 and may be seen to have almost no effect on the spectral response of the instrument.

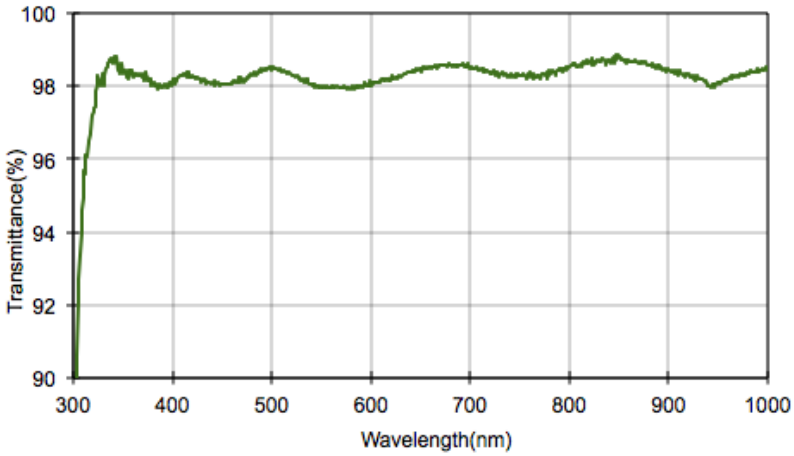

Figure 6: Absolute transmission of the IOO croystat window measured by the vendor after application of the anti-reflection coating.

4.2.3 Filters

High quality spectrophotometer measurements of all our filters were provided by the manufacturers and shown in Figure 7. Each filter is multiplied by the CCD QE and cryostat window transmission to give the total SED sensitivity of the instrument. The spectral response function of the telescope itself is then the only unknown and can be derived from the photometry.

	Filter Alone			Complete IO:O		
	λ_0	$\Delta\lambda$	FWHM	λ_0	$\Delta\lambda$	FWHM
u'	3479.2	548.9	675	3475.9	250.2	710
g'	4795.5	1299.6	1495	4852.5	970.8	1435
r'	6187.7	1224.8	1295	6197.4	1152.1	1285
i'	7658.7	1311.1	1385	7636.3	1188.3	1385
z'	-	-	-	9005.9	784.0	1030
B	4371.4	674.4	951	4415.8	434.0	973
V	5382.6	749.3	867	5397.9	647.2	890

Table 4: The effective central wavelength and effective width in Angstroms for each filter presented both for the filter itself and after correction for losses in the CCD QE and cryostat window. Also included is the passband full-width-at-half-maximum as a purely geometric description of the filter shape, though since the peak is never 100%, this contains no information about the absolute throughput of the filter. Values for z'-alone are undefined because it is a one-sided long-pass filter.

In Table 4 we present effective wavelengths and pass-band widths for each filter alone and that when convolved with the CCD QE and cryostat window transmission.

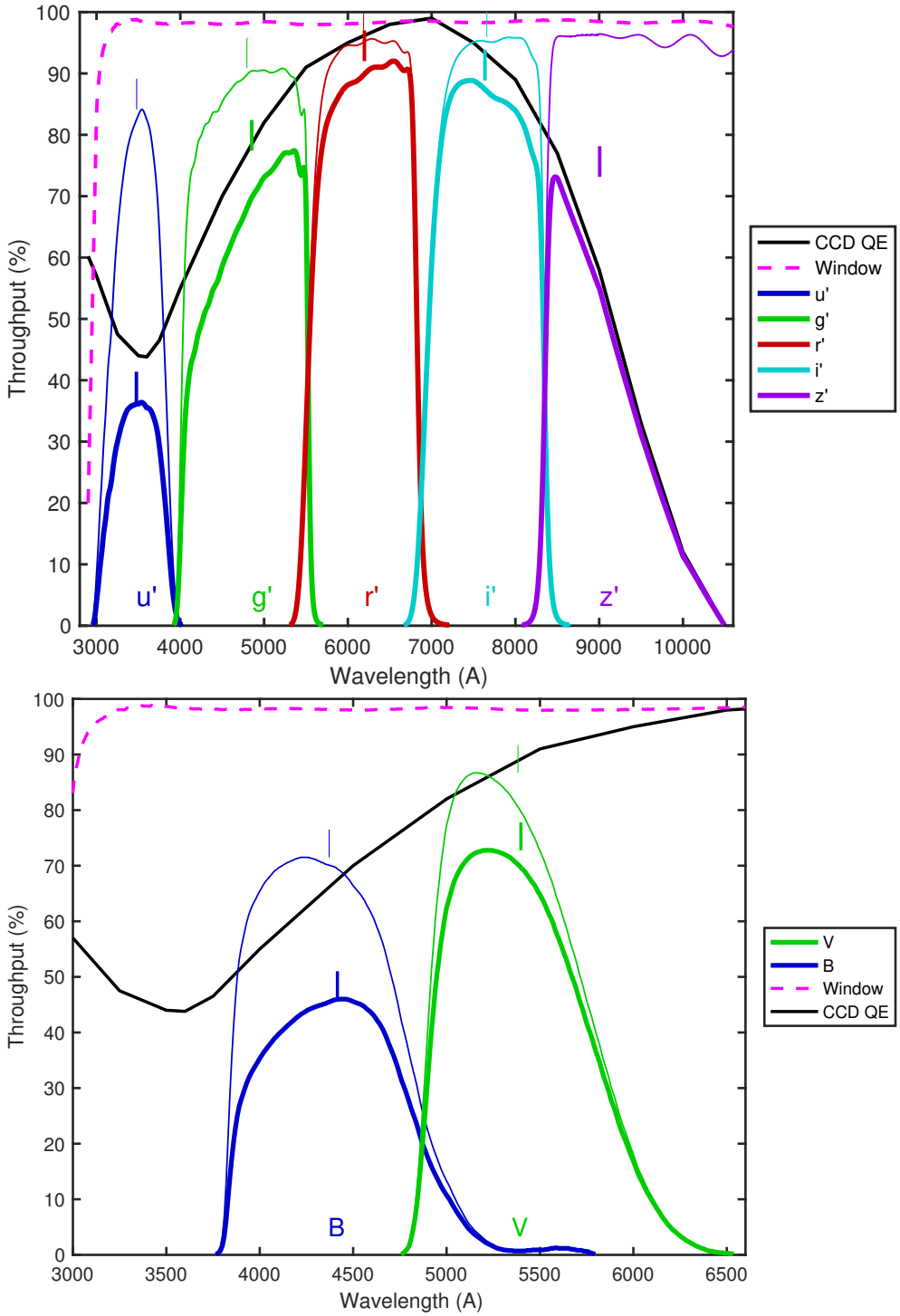

Figure 7: Transmission curves for the filters in IO:O. Thin lines are the measured transmission of the filters alone. The magenta line, essentially flat at 98% transmission, is a measurement of the cryostat window. The black curve is our model of the CCD QE. Thick lined filter traces are the product of all the above terms to give the effective spectral response of the entire instrument. The tick marks above each filter curve show the effective central wavelengths. The effective central wavelength of z' alone without the CCD is ill-defined and not shown.

5 Component and total transmissions

In Table 5 and Figure 8 we present the measured telescope throughput and modeled throughputs of each of the subsystem components numerically and graphically. Geometric collecting area and atmospheric extinction are accounted for in the measurement of the instrumental zero point. CCD QE, filter and cryostat window throughputs all contribute to the system's effective wavelength in the conversion from photon count to flux density. The residual discrepancy between the reference flux and the LT's natural zero point is the mirror reflectivity. The mean value of 76.4% in Table 5 implies two reflections each of 87.4%. Across the visible band, the theoretical maximum reflection for bare aluminium is in the range 89–92%.

For the CCD and cryostat window the throughput is reported as the ratio of the measured count rate to the count rate that would have been observed without that component's losses. This was derived by numerically integrating the models in Figure 7 over wavelength with and without each component included.

As a geometric description of the filter throughput and how it compares to a hypothetical, perfect top-hat filter, we quote the ratio of the effective width to the full width at half maximum. The 'Filter' and 'Total' data points for Bessell B, V fall substantially below the interpolation of the SDSS filters because of these filters' broader shape and lower peak transmission.

Correcting the measured telescope throughput for B, V, g', r', i', z' by the measured secular degradation, the results parallel the prediction for perfectly polished solid aluminium, offset by -4%. This small offset is unsurprising and may reflect either uncertainties in our measurement or a lower than theoretical coating efficiency.

	F_0^{ref} (Jy)	F_0^{LT} (Jy)	Telescope (%)	Filter (%)	CCD (%)	Window (%)	Total (%)	Atmos. (%)
u'	3767	2461	65.3	81.3	46.6	97.8	24.2	60.0
g'	3631	2850	78.5	86.9	76.1	98.2	51.0	86.0
r'	3631	2807	77.3	94.6	95.8	98.2	68.8	91.2
i'	3631	2642	72.8	94.7	92.1	98.4	62.4	95.5
z'	3565	2715	76.2	95.9	40.5	98.5	29.1	96.4
B	4130	3235	78.3	70.9	65.6	98.2	35.8	81.5
V	3781	2844	75.2	86.4	88.0	98.2	56.2	88.5

Table 5: F_0^{ref} is the reference zero magnitude flux above the atmosphere. This defines the AB magnitude scale for the Sloan-like filters and is a derived quantity for the B, V filters. 'Telescope' is the measured telescope throughput. Contributions of each component in the model are also given. Column 'Total' gives the end-to-end efficiency of LT-plus-IO:O compared to a 100% QE detector on a perfect $2.513\,\mathrm{m}^2$ telescope with hypothetical 100% transmission top-hat filters of the same FWHM as our actual filters. Zenith (airmass = 1) transmission through the atmosphere is included for comparison, but not included in the end-to-end system throughput estimate.

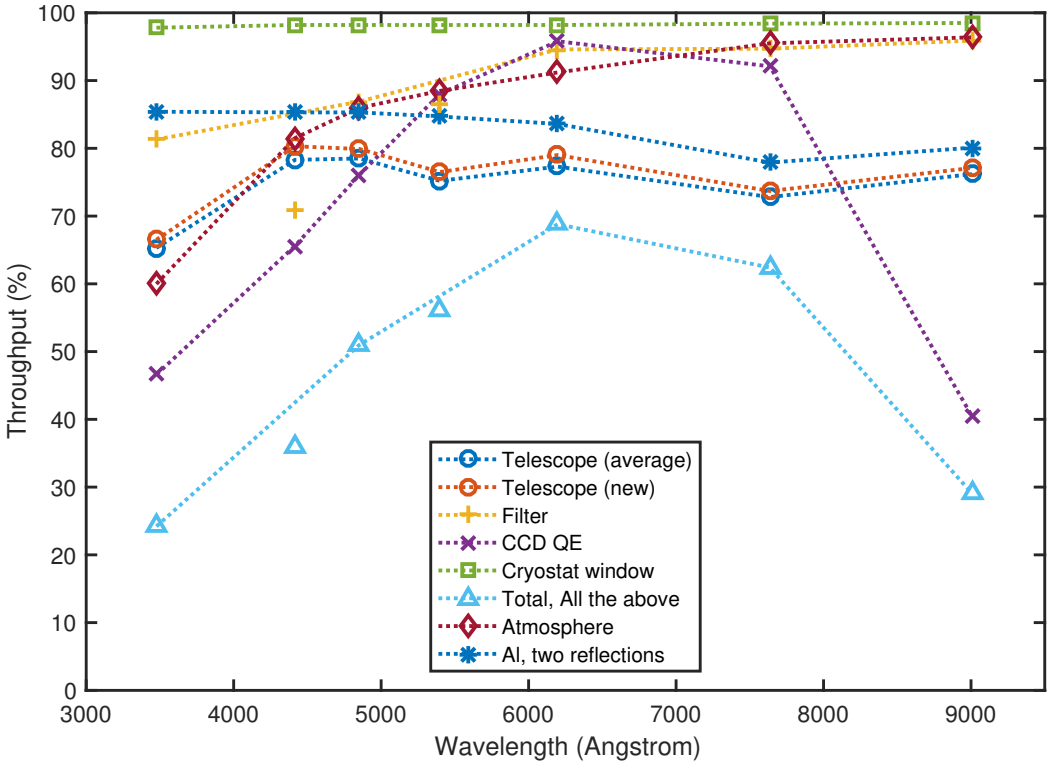

Figure 8: This plot shows the values tabulated in Table 5, the measured and modeled throughput of each system component. 'Telescope (average)' is derived from $\langle \mathrm{ZP} \rangle$ in Table 3 whereas 'Telescope (new)' estimates the throughput immediately after mirror re-coating, based on ZP_0.

6 Comparison to direct reflectance measurement

Direct measurements are occasionally taken of the LT primary mirror. Data are typically available only immediately following mirror re-coating when access to the mirror surface is readily available. We therefore recalculate the throughput values using ZP_0 instead of $\langle \mathrm{ZP} \rangle$ from Table 3. This gives an estimate for the telescope throughput with fresh mirror coatings. Since the reflectometer pass-bands do not perfectly match our photometric filters this offers only an approximate consistency check.

Wavelength (Å)	Reflectometer (%)	g' (%)	r' (%)	z' (%)	B (%)	V (%)	Bare Al (%)
4700	92.0	89.4	-	-	88.5	-	92.3
5300	90.5	89.4	-	-	-	86.7	92.1
6500	89.4	-	88.9	-	-	-	91.1
8800	82.8	-	-	86.8	-	-	89.0

Table 6: Reflectometer values are direct measurements from the primary mirror surface immediately after coating was performed. For the best matched LT filter we then present the single reflection efficiency inferred from the on-sky photometry. (Source of bare aluminium data : *Handbook of Optical Constants of Solids.* Edward D. Palik, ed., 1985, Academic Press.)

References

[1] Smith, Tucker, Kent et al., 2002, AJ, 123, 2121
[2] Eisenstein et al., 2006, ApJ, 167, 40
[3] J.A. Smith, private communication
[4] http://www-star.fnal.gov/NorthEqExtension_ugriz/index.html
[5] http://www.cadc-ccda.hia-iha.nrc-cnrc.gc.ca/en/community/STETSON/standards/
[6] Landolt, 1992, AJ, 104, 1
[7] Allen's Astrophysical Quantities, 4^{th} Edition, 2001
[8] Bessell, 1979, PASP, 91, 589
[9] Bertin & Arnouts, 1996, AAPS, 117, 393
[10] Magrath, 1997, PASP, 109, 303